

# Transport characterization of magnetic states in Superconductor/Ferromagnet Nb/Co multilayers

Olena M. Kapran<sup>1</sup>, Roman Morari<sup>2,3</sup>, Taras Golod<sup>1</sup>, Evgenii A. Borodianskyi<sup>1</sup>, Vladimir Boian<sup>2</sup>,  
Andrei Prepelita<sup>2</sup>, Nikolay Klenov<sup>3,4,5</sup>, Anatoli Sidorenko<sup>2,6</sup> and Vladimir M. Krasnov<sup>1,3\*</sup>

<sup>1</sup> *Department of Physics, Stockholm University, AlbaNova University Center, SE-10691 Stockholm, Sweden;*

<sup>2</sup> *Institute of Electronic Engineering and Nanotechnologies ASM, MD2028 Kishinev, Moldova;*

<sup>3</sup> *Moscow Institute of Physics and Technology, State University,  
9 Institutskiy per., Dolgoprudny, Moscow Region 141700 Russia;*

<sup>4</sup> *Lomonosov Moscow State University Skobeltsyn Institute of Nuclear Physics, Moscow, 119991, Russia;*

<sup>5</sup> *Moscow Technical University of Communication and Informatics (MTUCI), 111024 Moscow, Russia; and*

<sup>6</sup> *Laboratory of Functional Nanostructures, Orel State University named after I.S. Turgenev, 302026, Russia.*

Employment of the non-trivial proximity effect in Superconductor/Ferromagnet (S/F) heterostructures for creation of novel superconducting devices requires an accurate control of magnetic states in complex thin-film multilayers composing such devices. In this work we study experimentally in-plane transport properties of micro-structured Nb/Co multilayers. We apply various experimental techniques for characterization of multilayers, including the anisotropic magnetoresistance, the Hall effect and the first-order-reversal-curves analysis. We demonstrate that a combination of those techniques can provide a detailed knowledge of the magnetic state of the multilayer. In particular, we identify the range of existence of the coherently rotating, monodomain scissor-like state. It is anticipated, that in this noncollinear magnetic state the unconventional odd-frequency spin-triplet order parameter should appear. The non-hysteric nature of this state allows reversible tuning of the magnetic orientation. Thus, we identify the range of parameters and the procedure for controllable operation of devices based on such S/F heterostructures.

## I. INTRODUCTION

Competition between spin-polarized ferromagnetism and spin-singlet superconductivity leads to a variety of interesting phenomena including possible generation of the odd-frequency spin-triplet order parameter [1–3]. In recent years this exotic state has been extensively studied both theoretically [4–18] and experimentally [19–34] in various Superconductor/Ferromagnet (S/F) heterostructures. It is anticipated, that this phenomenon can be employed for creation of novel superconducting devices, in which supercurrent is determined and controlled by the magnetic state of the heterostructure, i.e., by the relative orientation of magnetizations in several F-layers [19, 20, 23, 24, 26–35].

However, practical realization of such devices is complicated because neither ways of controlling many degrees of freedom in S/F multilayers, nor even methods for monitoring the magnetic state in S/F micro- or nano-scale devices are established. The situation is complicated by a variety of coexisting phenomena in S/F heterostructures: (i) Both spin-singlet and spin triplet currents with short and long-range components can flow through the heterostructures [12]. Therefore, the supercurrent (even long-range) can not be automatically ascribed to the spin-triplet order. (ii) The supercurrent strongly depends on a usually unknown domain structure in F [24, 31, 36], flux quantization in S [37, 38], both influenced by the size and geometry. (iii) The long-range spin-triplet supercurrent appears only in the noncollinear magnetic state of S/F heterostructure [5, 9–12]. Therefore, utilization

of this phenomenon for device applications requires accurate determination and control of the micromagnetic state of micro- or nano-scale devices. A similar control is needed for operation of a large number of superconducting spintronics devices, including memory elements and spin valves [23, 30, 34, 39–43]. This non-trivial task of obtaining such the control using conventional transport characterization techniques is the main task of our work.

Here we study experimentally in-plane transport properties of micro-structured Nb/Co multilayers (ML's) with different number of layers and layer thicknesses. Our main goal is to demonstrate how conventional experimental techniques can be used for assessment of magnetic states of small S/F heterostructures and devices. We study the anisotropic magnetoresistance (MR), the Hall effect and the first-order-reversal-curves analysis (FORC) of MR. We demonstrate that a combination of those techniques, performed simultaneously, can provide a detailed knowledge of the magnetic configuration in the ML. In particular we can identify the parallel (P), the antiparallel (AP), the noncollinear monodomain scissor-like state and different polydomain states. Importantly, the scissor state corresponds to the noncollinear magnetic orientation of the ML, in which the unconventional odd-frequency spin-triplet order parameter should appear. The non-hysteric nature of this state allows reversible tuning of the magnetic configuration. Thus, we identify the range of parameters and the procedure for controllable operation of devices based on S/F heterostructures.

The paper is organized as follows. In section II we describe sample fabrication and layout. In section III

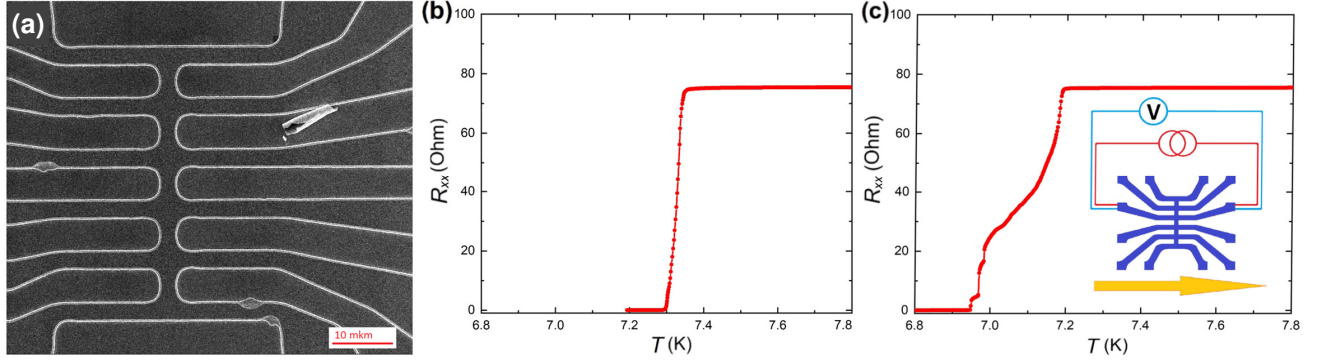


FIG. 1. (color online). (a) SEM image (top view) of a micro-patterned Nb/Co multilayer. The sample contains 12 contacts and several horizontal and vertical bridges with the width of few microns. The multiterminal configuration allows simultaneous measurements of longitudinal and Hall resistances in the four-probe configuration. Panels (b) and (c) show temperature dependencies of the longitudinal resistance  $R_{xx}$  for the same horizontal bridge #3 on a Nb(50 nm)/[Co(1.5 nm)/Nb(6 nm)/Co(2.5 nm)/Nb(6 nm)]<sub>3</sub>Co(1.5 nm)/Nb(6 nm)/Si ML. Inset in (c) shows a sketch of the contact configuration. Measurements are made under the same experimental conditions (at zero applied field) but for different prehistories: the curve in (b) is obtained after zero-field cooling, while the curve in (c) after application of a demagnetizing field sequence  $\pm 0.02$  T at low  $T$ . The yellow arrow in the inset indicates the direction of positive demagnetizing field.

main experimental results are presented, including: A. Memory (prehistory) effect on longitudinal resistance; B. Non-linear flux-flow Hall effect, C. Longitudinal and Hall MR, D. Anisotropic MR in the normal state and E. First-order-reversal-curves analysis of MR, followed by Discussion and Conclusions.

## II. SAMPLES

We study Nb/Co multilayers with different number of layers and layer thicknesses. The ML's are deposited by magnetron sputtering in a single deposition cycle. The system allows switching between several targets without depressurization of the chamber. We use a niobium target (99.95 % purity) for S-layers (Cooper pair generators) and as thin interlayer spacers between F-layers, a cobalt target (99.95 % purity) for deposition of F-layers, and a pure silicon target (99.999 %) for deposition of seeding bottom layers and protective top layers to prevent structure oxidation. ML's are grown on commercial (1 1 1) oriented silicon wafers. Prior to deposition, targets were precleaned by plasma-etching process for 3 minutes before starting the deposition cycle and in addition for 1 minute upon switching between targets. The deposition is performed at room temperature and with water cooled sample stage. Films thicknesses are defined using the pre-calibrated growth rates: 3.5 nm/s for niobium and 0.1 nm/s for cobalt films.

For every set of layers, three identical samples were prepared simultaneously, of which some were used for calibration of films etching rates during further processing. ML's are patterned into micron-scale bridges with multiple contacts using photolithography and reactive

ion etching. Scanning electron microscope (SEM) image of one of the studied samples is shown in Fig. 1 (a). Multi-terminal geometry of samples allows simultaneous four-probe measurements of different segments of the sample in both longitudinal and transverse directions. Resistances are measured by the lock-in technique. More details about fabrication, characterization and experimental setup can be found elsewhere [24, 34, 43].

## III. RESULTS

Measurements are performed in a closed-cycle <sup>3</sup>He cryostat with a superconducting magnet. In all cases magnetic field is applied parallel to the film plane. Below we present results for two ML's with layer compositions (bottom -to -top) Nb(50 nm)/Co(1.5 nm)/Nb(8 nm)/Co(2.5 nm)/Nb(8 nm)/Si and Nb(50 nm)/[Co(1.5 nm)/Nb(6 nm)/Co(2.5 nm)/Nb(6 nm)]<sub>3</sub>Co(1.5 nm)/Nb(6 nm)/Si (the subscript 3 indicates that the structure in the square brackets is repeated sequentially 3 times)

### III A. Memory (prehistory) effect

Figures 1 (b,c) show measured temperature dependencies of the longitudinal resistance  $R_{xx}(T)$  for one of the bridges on a Nb(50 nm)/[Co(1.5 nm)/Nb(6 nm)/Co(2.5 nm)/Nb(6 nm)]<sub>3</sub>Co(1.5 nm)/Nb(6 nm)/Si ML at zero applied field. Resistances are measured with a small ac-current amplitude  $I_{ac} = 1 \mu\text{A}$ . A schematic representation of the structure and the contact configuration is shown in the inset in Fig. 1 (c). The curves in (b) and

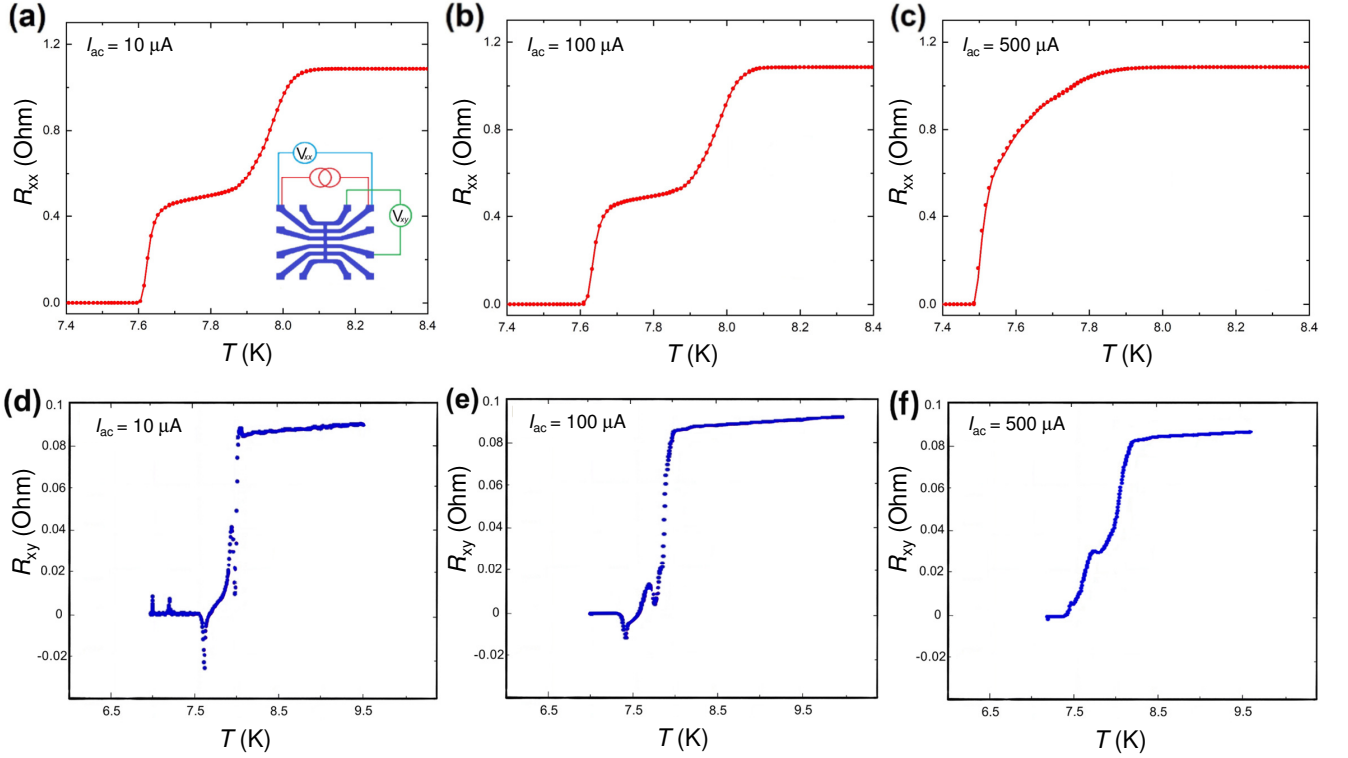


FIG. 2. (color online). Temperature dependencies of longitudinal (top row a-c) and Hall (bottom row d-f) resistances measured at different bias currents for the same segment of a Nb(50 nm)/Co(1.5 nm)/Nb(8 nm)/Co(2.5 nm)/Nb(8 nm)/Si ML at zero applied field and with the same magnetic prehistory.  $R_{xx}$  and  $R_{xy}$  are measured simultaneously at different ac current amplitudes (a,d)  $10\mu\text{A}$ , (b,e)  $100\mu\text{A}$ , (c,f)  $500\mu\text{A}$ . Contact configuration is shown in the inset in (a). The non-linear (bias-dependent)  $R_{xx}$  and  $R_{xy}$  in the transition region indicates flux-flow nature of resistances.

(c) are quite different, although they are measured at the same bridge under the the same experimental conditions (zero field,  $I_{ac} = 1\mu\text{A}$ ). However, these measurements have different prehistories.

The curve in Fig. 1 (b) was obtained immediately after zero-field cooling. It shows a sharp transition at  $T \simeq 7.3$  K, indicating that superconductivity in the whole structure appears simultaneously. The curve in Fig. 1 (c) is measured after applying a demagnetizing alternating magnetic field at  $T \sim 3$  K, decaying from  $\pm 0.02$  T to zero. It is seen that despite the same measurement conditions, the  $R_{xx}(T)$  curves in Figs. 1 (b) and (c) are significantly different. In particular, an additional broad shoulder develops in  $R_{xx}(T)$  in Fig. 1 (c) in the range  $6.9\text{ K} < T < 7.2\text{ K}$ . This clearly reveals the memory effect: properties of the ML depend on magnetic prehistory. This in turn indicates that superconducting properties of the ML bridge depend of the particular magnetic state of the ML established after remagnetization of the sample.

### III B. Non-linear flux-flow Hall effect

Figure 2 shows temperature dependencies of longitudinal  $R_{xx}$  (top panels a-c) and Hall  $R_{xy}$  (bottom panels d-f) resistances measured at a ML bridge Nb(50 nm)/Co(1.5 nm)/Nb(8 nm)/Co(2.5 nm)/Nb(8 nm)/Si.  $R_{xx}$  and  $R_{xy}$  are measured simultaneously. The curves are obtained using the same contact configuration, sketched in the inset of Fig. 2 (a), and the same prehistory, without changing magnetic field,  $H = 0$ , and the state of the ML. However, measurements are made with different ac-current amplitudes  $I_{ac}$  (a,d)  $10\mu\text{A}$ , (b,e)  $100\mu\text{A}$ , (c,f)  $500\mu\text{A}$ .

We observe that at low and intermediate bias currents, Figs. 2 (a,b), the main resistive transition occurs at  $T \simeq 8\text{K}$ , corresponding to the superconducting critical temperature of the bottom 50 nm thick Nb layer. At lower  $T = 7.6 - 7.9\text{ K}$  there is a shoulder in  $R_{xx}$  originating from 8 nm thin Nb interlayers between F-layers. As described in the previous section, this shoulder exhibits a memory effect, see Figs. 1 (b) and (c). However, for measurements in Fig. 2 the magnetic prehistory has not been changed and the shoulder in Figs. 2 (a,b) is unchanged. At high bias, Fig. 2 (c) the resistive transition

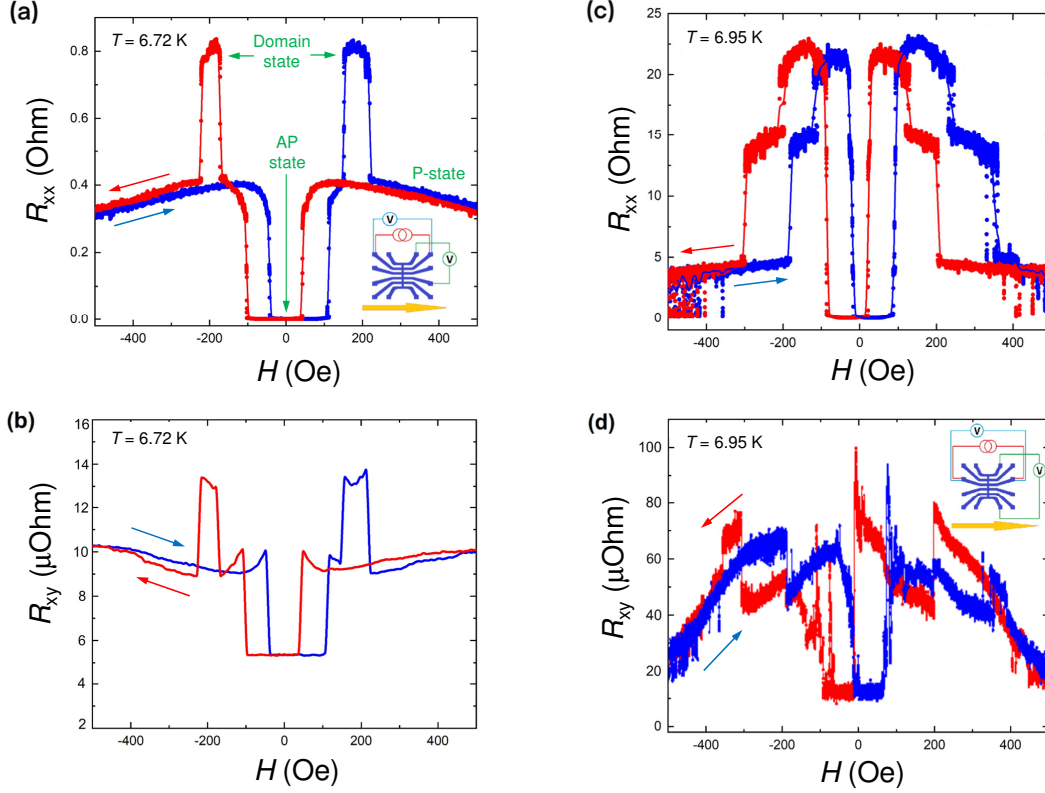


FIG. 3. (color online). Longitudinal (a,c) and Hall (b,d) magnetoresistances for the Nb(50 nm)/[Co(1.5 nm)/Nb(6 nm)/Co(2.5 nm)/Nb(6 nm)]<sub>3</sub>Co(1.5 nm)/Nb(6 nm)/Si sample. Measurements are done at temperatures corresponding to the shoulder regions in  $R_{xx}(T)$  for these bridges. Insets in (a) and (d) show contact configurations and the positive field direction (yellow arrows). Blue and red curves represent up and down field sweeps, respectively. Three distinct magnetic states can be identified: The P-state corresponds to the high field state with an intermediate  $R_{xx}$  value, the state with  $R_{xx} = 0$  at low fields corresponds to the AP-state, and the high-resistance state in-between, to the domain state. Note, that a flux-flow Hall effect appears in the domain state, compare panels (a) and (b) and (c) and (d).

is smeared out due to flux-flow phenomenon, i.e., motion of depinned Abrikosov vortices [44–46].

The key observation from Figs. 2 (d,e,f) is that the Hall resistance within the shoulder region is non-linear, i.e., it depends strongly on the bias current, while above the shoulder, in the normal state it is linear, i.e. independent of bias [47]. At low bias and intermediate bias, Figs. 2 (d,e),  $R_{xy}$  changes sign within the shoulder. Such a behavior is typical for the flux-flow type Hall effect in superconductors [44, 45]. The bias current exerts a Lorentz force on Abrikosov vortices. At low bias just above the depinning current, vortices are moving with a small velocity along the Lorentz in the direction perpendicular to the current and generate the longitudinal flux-flow resistance. The Hall resistance in this case is determined by small deviations of the vortex path and, therefore, may easily acquire different signs. With increasing bias, the vortex velocity increases, leading to appearance of the Magnus force moving vortices in the direction parallel to the current, and thus contributing significantly to the Hall resistance. At a very large bias, vortices are

supposed to be dragged along the current [46], thus generating the Hall signal similar to the longitudinal signal at low bias. This is qualitatively consistent with our observations. At large bias  $I = 500 \mu\text{A}$  in Fig. 2 (f) the shape  $R_{xy}(T)$  clearly resembles  $R_{xx}(T)$  from Fig. 2 (a). Therefore, observations of the bias-dependent non-linear Hall effect at the shoulder unambiguously proves the flux-flow origin of this shoulder. The non-linearity is caused by the strong bias dependence of the vortex velocity in the vicinity of the depinning current [45].

Since measurements are done at  $H = 0$ , a relevant question is where from do vortices appear. As discussed above, the shoulder region exhibits rich magnetic pre-history, most likely caused by rearrangement of magnetic domains in the ML. Therefore, it is natural to assume that vortices are induced by domain walls in F-layers, which create out-of-plane field component, sufficient for creation of vortices [48–51]. Below we will provide additional experimental data that confirm this scenario.

### III C. Longitudinal and Hall magnetoresistances

Figures 3 (a) and (c) show field dependencies of longitudinal resistances  $R_{xx}(H)$  for two segments of the Nb(50 nm)/[Co(1.5 nm)/Nb(6 nm)/Co(2.5 nm)/Nb(6 nm)]<sub>3</sub>Co(1.5 nm)/Nb(6 nm)/Si ML. Measurements are done at  $T = 6.72$  K and 6.95 K, respectively, corresponding to the beginning and the end of the shoulder in the  $R_{xx}(T)$  curve, see Fig. 1 (c), which explains the difference in absolute values of  $R_{xx}$ . Up (blue) and down (red) field sweeps are shown. The hysteresis of magnetoresistance,  $R_{xx}(H)$ , reflects the change of the magnetization state of the ML. We can distinguish several magnetic states. The state at high field with an intermediate  $R_{xx}$  value apparently corresponds to the P-state of the ML. The  $R_{xx} = 0$  state in the middle - to the AP state, at which the superconductivity is expected to be the strongest due to partial cancellation of exchange fields from neighbor F-layers [4–6, 8–10]. Finally, there are one, Fig. 3 (a), or several, Fig. 3 (b), high resistance states in-between P and AP states. The origin of those states is less obvious.

Figs. 3 (c) and (d) represent field dependencies of Hall resistances measured simultaneously [47]. In all cases there is a negligible Hall signal for the case  $R_{xx} = 0$ , confirming that this is the AP-state with cancelled fields. But, there are clear Hall signals in the high-resistive states. As follows from the previous section, such the Hall signal is associated with vortices in S-layers, which are oriented perpendicular to the film, and are likely created by domain walls in F-layers pinching stray magnetic fields through S-layers [48–51]. The domain origin of this high-resistive state is consistent with the observed pre-history effect in the shoulder region, Figs. 1 (b) and (c), and is further confirmed below.

### III D. Anisotropic magnetoresistance in the normal state

Fig. 4 (a) shows longitudinal MR in the normal state at  $T = 9$  K  $> T_c$  for a micro-bridge from the Nb(50 nm)/Co(1.5 nm)/Nb(8 nm)/Co(2.5 nm)/Nb(8 nm)/Si ML. Small but distinct hysteretic maxima in  $R_{xx}(H)$  for up and down field sweeps can be seen at  $H \simeq \pm(100 - 150)$  Oe. The smallness of MR is caused by (i) shunting of the ferromagnetic response by the thick bottom Nb layer (50 nm) and (ii) by relatively thick Nb spacers (8 nm) which lead to small exchange coupling between F-layers. There can be two explanations for the observed maxima. First, it could be the anisotropic magnetoresistance (AMR), which exists even in a single F-layer and is associated with appearance of domains, misaligned with respect to bias current [52]. Maxima of AMR occur at the perpendicular orientation of magnetization and current. Second, could be the giant MR,

which appears only in coupled spin-valve-type ML's with maxima in the AP state.

Due to shunting of the ferromagnetic response by Nb layers, it is difficult to distinguish the two mechanisms just by looking at the amplitude and the shape of MR. However, we can compare characteristic fields with those observed from MR below  $T_c$ , which is shown in Fig. 4 (c) for the same bridge. It is seen that both above and below  $T_c$  the magnetic saturation occurs at  $H_s \simeq 300$  Oe. At higher fields the ML is in the monodomain P-state. Transition to the AP state, corresponding to  $R_{xx} = 0$  in Fig. 4 (c), occurs at very small fields, close to zero, consistent with the coercive field value  $H_C \simeq 30$  Oe deduced for similar unpatterned ML's films earlier [43]. Maxima of  $R_{xx}(H)$  below  $T_c$  occur at  $H \simeq \pm(200 - 250)$  Oe, which is only slightly larger than in the normal state, Fig. 4 (a). The field enhancement can be explained by the screening effect from superconducting Nb spacer layers [48] and is consistent with earlier observations of such a phenomenon [52]. Therefore, the field of maximal normal MR seems to be larger than the field range of the AP state. This implies that the peaks in the normal state MR are more likely caused by the AMR, rather than GMR. Such a conclusion is consistent with results from Ref. [52] and is also supported by observation of the flux-flow Hall effect at the maxima  $R_{xx}(H)$  in the superconducting state, which we associated with domains that in turn cause appearance of AMR.

### III E. First-order-reversal-curves analysis of magnetoresistance

The first-order-reversal-curves (FORC) analysis is a powerful tool for *in-situ* characterization of magnetic states in complex ferromagnetic structures [53–55]. FORC analysis starts at the same saturated state. Then field is swept to a reversal field  $H_r$  and measurements are carried out on the way back to the saturated state. The experiment is repeated with gradually varying  $H_r$ . Recently it has been shown that FORC can be used for the analysis of magnetic states in S/F ML's [34]. Essentially we have to search for appearance of different types of hysteresis in the FORC response, which indicate switching into some specific magnetic states. There are two mechanisms for appearance of hysteresis in the ML's [34, 37]. The major hysteresis is associated with switching in and out from the magnetostatically stable AP state. Multiple smaller ones are associated with switching between different domain states, which are also metastable.

Figs. 4 (d-i) represent FORC analysis of longitudinal MR  $R_{xx}(H)$  for the same micro-bridge. Magnetic field is swept from above the saturation field  $H = +500$  Oe down to the reversal field  $H_r$  and back to the saturation field. Red lines represent forward curves and blue - the FORC's. In Fig. 4 (d)  $H_r \simeq +30$  Oe and the

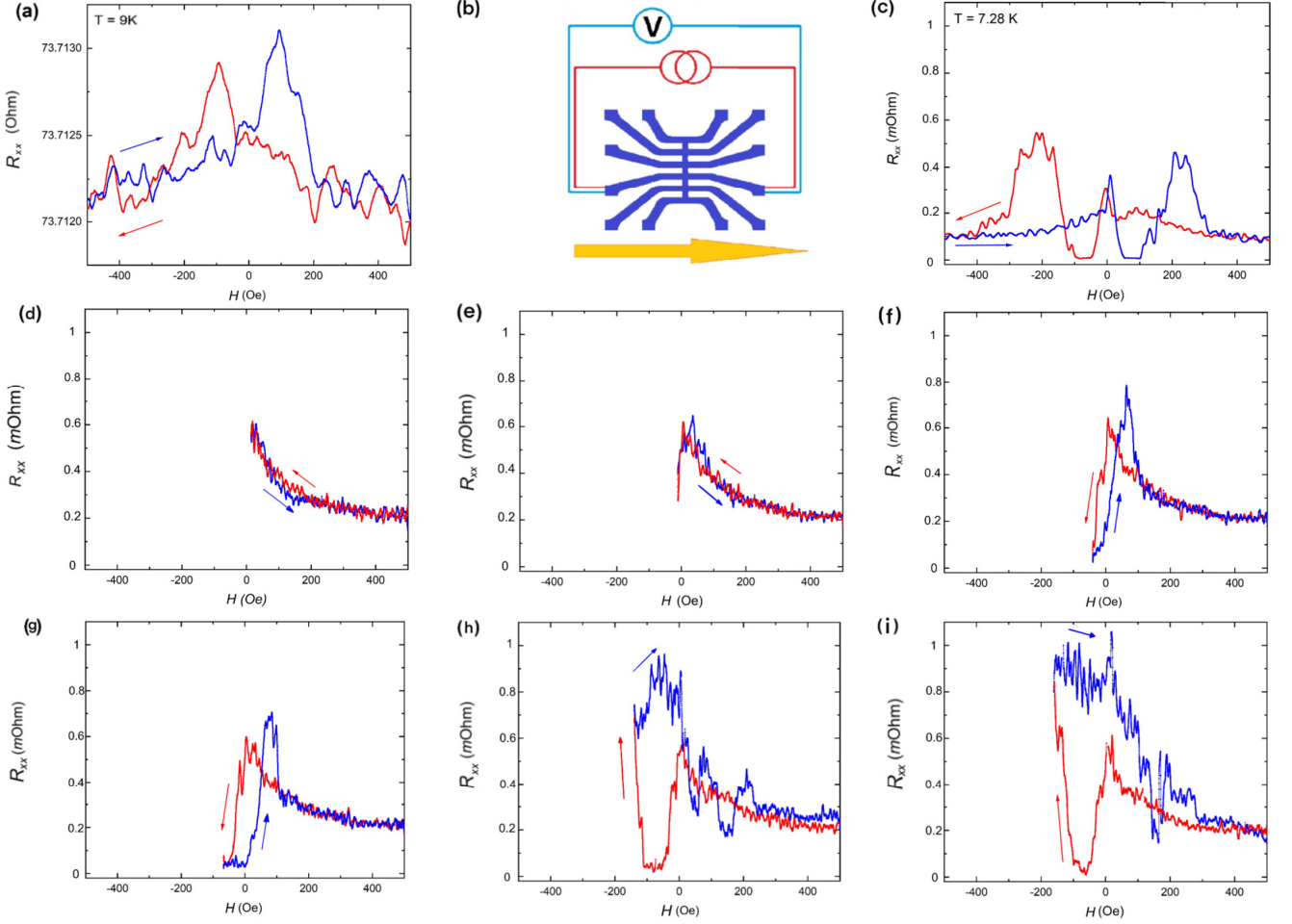


FIG. 4. (color online). Magnetoresistance of a bridge on the Nb(50 nm)/Co(1.5 nm)/Nb(8 nm)/Co(2.5 nm)/Nb(8 nm)/Si sample. (a) Normal state MR at  $T = 9$  K. Red and blue curves represent downward and upward field sweeps, respectively. (b) A sketch of the contact configuration. (c-i) FORC analysis of magnetoresistances in the superconducting state at  $T = 7.28$  K: (c) full range MR, (d-i) FORC's with sequentially decreasing reversal fields  $H_r$ . Development of hysteresis with changing  $H_r$  allows identification of magnetic states. Initially the MR is reversible (d,e) indicating scissor-like coherent rotation from P to AP state. The first hysteresis appears upon switching to the AP state  $R_{xx} \simeq 0$  (f,g). A second hysteresis with high  $R_{xx}$  appears after switching from the AP state to the domain state (h,i).

FORC is reversible. The non-hysteretic behavior corresponds to coherent monodomain rotation of magnetization in neighbor layers in a scissor-like manner [34, 37]. In Fig. 4 (e)  $H_r = 0$  and the FORC starts to show a tiny hysteresis, which vanishes at  $H > 50$  Oe. In Fig. 4 (f)  $H_r \simeq -25$  Oe here the forward (red) curve almost reached zero resistance, characteristic for the AP state, and the reversal curve (blue) shows a clear hysteresis. In Fig. 4 (g)  $H_r \simeq -50$  Oe is in the middle of the  $R_{xx} = 0$  minimum. The hysteresis of the reversal curve is, however, identical to that in Fig. 4 (f), which shows that the state of the ML remains the same. As reported in Ref. [34] appearance of the initial hysteresis at small fields is often associated with switching to the AP state. This is fully consistent with our observation that the initial hysteresis corresponds to the minimum longitudinal

resistance of the ML.

In Fig. 4 (h)  $H_r \simeq -150$  Oe at the upturn of  $R_{xx}(H)$  beyond the AP minimum. Now the reversal curve has clearly changed with respect to Figs. 4 (f,g), indicating switching into a different state. Furthermore the range of hysteresis has expanded to  $H > 200$  Oe and several additional small switches occur within this range. In Fig. 4 (i)  $H_r$  is in the middle of the maximum. The reversal curve is clearly different from that in Fig. 4 (h), revealing yet another initial state. With further increase of  $H_r$  towards the negative saturation field, the hysteresis changes gradually until reaching the saturated state, shown in Fig. 4 (c). Such a gradual transformation indicates that the ML is in a poly-domain state with many metastable states.

Thus, from FORC analysis we conclude that upon re-



magnetization of the ML from the P-state, it first enters into a coherently rotating, nonhysteretic, scissor state, after which it abruptly switches into the AP state, stays in it for a while and then breaks into a poly-domain state, which gradually turn into the opposite P-state. This picture is fully consistent with the assessment based on Hall effect analysis and with earlier FORC analysis of Ni-based  $\text{SF}_1\text{NF}_2\text{S}$  spin valves made in Ref. [34].

#### IV. DISCUSSION

The reported here effect of switching from P to AP state in S/F heterostructures is well known [21, 33–35] and explained [4–6, 8–10]. In the P state exchange fields from neighbor F layers add up, leading to a suppression of superconductivity. In the AP the exchange fields subtract, leading to an enhancement of superconductivity. Therefore, P and AP states should correspond to high and low resistances, respectively. The P state occurs at high fields above the saturation field. Therefore, switching from P to AP state, upon reduction of field, leads to reduction of resistance, see Figs. 3 (a,c) and 4 (f,g). However, in this work we observed that upon remagnetization of the ML's from AP to P state, yet another state with resistance *higher* than in the P-state appears, see Fig. 3. This state depends on prehistory and causes an additional shoulder in the resistive transition of the ML, Fig. 1. Interpretation of this high-resistive state is less straightforward because it can not be explained solely by the ferromagnetic response of the ML.

From the analysis of the Hall effect, Fig. 2, we concluded that the high resistive state is associated with the flux-flow phenomenon in the ML. Presence and motion of Abrikosov vortices in S-layers increases the overall resistance above that in a vortex-free P-state. FORC analysis, Fig. 4, demonstrated that the high-resistance state is split in many small hysteresis steps. This allows identification of this state as a poly-domain state. Most likely, Abrikosov vortices are introduced by domain walls with out-of-plane magnetic field component. This is consistent with observation of the AMR phenomenon in S/F and F/S/F heterostructures, made previously [52].

Generally, the poly-domain state is unwanted in most devices based on S/F heterostructures because it is hard to control. Domains cause an irreversible behavior of the heterostructure, associated with both the magnetic hysteresis and with generation of Abrikosov vortices, which are pinned at film defects. As shown previously [24], those two factors may dramatically distort characteristics of S/F devices.

FORC analysis allows a clear distinction of poly- and mono-domain states in complex magnetic systems [53–55], including S/F heterostructures. In Ref. [34] this was demonstrated using out-of-plane measurements. Here we show that a similar information can be obtained us-

ing in-plane transport measurements, see Figs. 4 (c-i). From those measurements we can characterize evolution of micromagnetic states in our structures upon remagnetization. We observe that the switching from parallel to anti-parallel state occurs in a mono-domain manner via reversible coherent rotation, see Figs. 4 (d,e). Micromagnetic simulations demonstrate that this is a scissor-like state with a gradual rotation of magnetizations in neighbor F-layers in opposite directions [34, 37]. On the other hand, switching from AP to P state occurs by splitting into domains [34]. This leads to appearance of the irreversible high resistive state with Abrikosov vortices, nonlinear Hall effect and prehistory dependence.

The nonhysteretic scissor-like state is most interesting from the point of view of device applications because it allows controllable and reversible variation of the magnetic state of the heterostructure. Moreover, this state corresponds to the noncollinear magnetic state of the ML at which the unconventional odd-frequency spin triplet component of the supercurrent is expected to be induced, which is central for operation of various devices. Therefore, the technique, developed in this work, allows identification of the range of parameters and the procedure for controllable operation of devices based on S/F heterostructures. This is the main result of our work.

#### CONCLUSIONS

To conclude, we have studied experimentally in-plane transport properties of micro-structured Nb/Co multilayers with different layer composition. We have demonstrated how conventional transport techniques can be used for assessment of magnetic states of small S/F heterostructures and devices. For this we apply various experimental techniques, including the anisotropic magnetoresistance, the Hall effect and the first-order-reversal-curves analysis. We have shown that a combination of those techniques, performed simultaneously, can provide a detailed knowledge of the micro-magnetic state of S/F multilayers. We have identified the parallel, the antiparallel, the mono-domain scissor-like state and a set of poly-domain states. Importantly, the scissor state corresponds to the noncollinear magnetic state of the multilayer in which the unconventional odd-frequency spin-triplet order parameter should appear in the heterostructure. The non-hysteretic nature of this state allows controllable tuning of magnetic orientation. Thus, we identify the range of parameters and the procedure for controllable operation of superconducting spintronic devices based on S/F heterostructures. Essentially we conclude that for moderately small (micrometer-scale) devices controllable and highly reversible operation can be achieved at fields between one of the P-states down to the AP state without entering into the realm of the opposite P state.

## Acknowledgments

We are grateful to Sergey Bakurskiy, Igor Soloviev, Andrey Schegolev, Yury Khaydukov, Mikhail Kupriyanov and Alexander Golubov for stimulating discussions. The work was supported by the European Union H2020-WIDESPREAD-05-2017-Twinning project “SPINTECH” under grant agreement Nr. 810144 (R.M., O.M.K., V.B., A.S., V.M.K., sample preparation and low temperature measurements), partially by the project STCU #6329 “Full switching memory element for spintronics on the base of superconducting spin-valve effect” and the Russian Science Foundation grant No. 19-19-00594 (V.M.K.: data analysis and manuscript preparation). The manuscript was written during a sabbatical semester of V.M.K. at MIPT, supported by the Faculty of Natural Sciences at SU and the Russian Ministry of Education and Science within the program “5top100”. V.M.K. is grateful to MIPT for the hospitality.

---

\* E-mail: Vladimir.Krasnov@fysik.su.se

- [1] A. I. Buzdin, A. V. Vedyayev, and N. V. Ryzhanova, Spin-orientation-dependent superconductivity in F/S/F structures. *Europhys. Lett.* **54**, 686-691 (1999).
- [2] A. Kadigrobov, R. I. Shekhter, and M. Jonson, Quantum spin fluctuations as a source of long-range proximity effects in diffusive ferromagnet-superconductor structures. *Europhys. Lett.* **48**, 394-400 (2001).
- [3] F. S. Bergeret, A. F. Volkov, and K. B. Efetov, Long-range proximity effects in superconductor-ferromagnet structures. *Phys. Rev. Lett.* **86**, 4096-4099 (2001).
- [4] A. I. Buzdin, Proximity effects in superconductor-ferromagnet heterostructures. *Rev. Mod. Phys.* **77**, 935-976 (2005).
- [5] F. S. Bergeret, A. F. Volkov, and K. B. Efetov, Odd triplet superconductivity and related phenomena in superconductor-ferromagnet structures. *Rev. Mod. Phys.* **77**, 1321-1373 (2005).
- [6] Ya. V. Fominov, A. A. Golubov, T. Yu. Karminskaya, M. Yu. Kupriyanov, R. G. Deminov, and L. R. Tagirov, Superconducting Triplet Spin Valve. *JETP Lett.* **91**, 308 (2010).
- [7] Ya. M. Blanter and F. W. J. Hekking, Supercurrent in long SFFS junctions with antiparallel domain configuration. *Phys. Rev. B* **69**, 024525 (2004).
- [8] M. Eschrig, Spin-polarized supercurrents for spintronics: a review of current progress. *Rev. Prog. Phys.* **78**, 104501 (2015).
- [9] M. Houzet and A. I. Buzdin, Long range triplet Josephson effect through a ferromagnetic trilayer. *Phys. Rev. B* **76**, 060504(R) (2007).
- [10] Y. Asano, Y. Sawa, Y. Tanaka, and A. A. Golubov, Odd triplet superconductivity and related phenomena in superconductor-ferromagnet structures. *Phys. Rev. B* **76**, 224525 (2007).
- [11] L. Trifunovic, Z. Popovic, and Z. Radovic, Josephson effect and spin-triplet pairing correlations in SF1F2S junctions. *Phys. Rev. B* **84**, 064511 (2011).
- [12] A. S. Mel'nikov, A. V. Samokhvalov, S. M. Kuznetsova, and A. I. Buzdin, Interference Phenomena and Long-Range Proximity Effect in Clean Superconductor-Ferromagnet Systems. *Phys. Rev. Lett.* **109**, 237006 (2012).
- [13] N. G. Pugach, and A. I. Buzdin, Magnetic moment manipulation by triplet Josephson current. *Appl. Rev. Lett.* **101**, 242602 (2012).
- [14] M. Alidoust, G. Sewell, and J. Linder, Non-Fraunhofer Interference Pattern in Inhomogeneous Ferromagnetic Josephson Junctions *Phys. Rev. Lett.* **108**, 037001 (2012).
- [15] C. Richard, A. Buzdin, M. Houzet, and J. S. Meyer, Signatures of odd-frequency correlations in the Josephson current of superconductor/ferromagnet hybrid junctions, *Phys. Rev. B* **92**, 094509 (2015).
- [16] S. Hikino and S. Yunoki, Magnetization induced by odd-frequency spin-triplet Cooper pairs in a Josephson junction with metallic trilayers. *Phys. Rev. B* **92**, 024512 (2015).
- [17] J. Linder and J. W. A. Robinson, Superconducting spintronics. *Nature Phys.* **11**, 307 (2015).
- [18] H. Meng, J. Wu, X. Wu, M. Ren, and Y. Ren, Long-range superharmonic Josephson current and spin-triplet pairing correlations in a junction with ferromagnetic bilayers. *Sci. Rep.* **6**, 21308 (2016).
- [19] C. Bell, G. Burnell, C. W. Leung, E. J. Tarte, D.-J. Kang, and M. G. Blamire, Controllable Josephson current through a pseudospin-valve structure. *Appl. Rev. Lett.* **84**, 1153-1155 (2004).
- [20] J. W. A. Robinson, G. B. Halász, A. I. Buzdin, and M. G. Blamire, Enhanced Supercurrents in Josephson Junctions Containing Nonparallel Ferromagnetic Domains, *Phys. Rev. Lett.* **104**, 207001 (2010).
- [21] P. V. Leksin, N. N. Garif'yanov, I. A. Garifullin, J. Schumann, V. Kataev, O. G. Schmidt, and B. Büchner, Manifestation of New Interference Effects in a Superconductor-Ferromagnet Spin Valve. *Phys. Rev. Lett.* **106**, 067005 (2011).
- [22] V. I. Zdravkov, J. Kehrle, G. Obermeier, D. Lenk, H.-A. K. von Nidda, C. Mueller, M. Y. Kupriyanov, A. S. Sidorenko, S. Horn, R. Tidecks, and L. R. Tagirov, Experimental observation of the triplet spin-valve effect in a superconductor-ferromagnet heterostructure. *Phys. Rev. B* **87**, 144507 (2013).
- [23] B. Baek, W. H. Rippard, S. P. Benz, S. E. Russek, and P. D. Dresselhaus, Hybrid superconducting-magnetic memory device using competing order parameters *Nat. Commun.* **5**, 3888 (2014).
- [24] A. Iovan, T. Golod, and V. M. Krasnov, Controllable generation of a spin-triplet supercurrent in a Josephson spin valve, *Phys. Rev. B* **90**, 134514 (2014).
- [25] Yu. N. Khaydukov, G. A. Ovsyannikov, A. E. Sheyerman, K. Y. Constantinian, L. Mustafa, T. Keller, M. A. Uribe-Laverde, Yu. V. Kislinskii, A. V. Shadrin, A. Kalaboukhov, B. Keimer, and D. Winkler, Evidence for spin-triplet superconducting correlations in metal-oxide heterostructures with noncollinear magnetization, *Phys. Rev. B* **90**, 035130 (2014).
- [26] J. W. A. Robinson, J. D. S. Witt, and M. G. Blamire, Controlled Injection of Spin-Triplet Supercurrents into a Strong Ferromagnet, *Science* **329**, 59 (2010).



- [27] T.S. Khaire, M.A. Khasawneh, W.P. Pratt, Jr., and N.O. Birge, Observation of Spin-Triplet Superconductivity in Co-Based Josephson Junctions. *Phys. Rev. Lett.* **104**, 137002 (2010).
- [28] N. Banerjee, J.W.A. Robinson and M.G. Blamire, Reversible control of spin-polarized supercurrents in ferromagnetic Josephson junctions. *Nature Commun.* **5**, 4771 (2014).
- [29] W. M. Martinez, W. P. Pratt, Jr., and N. O. Birge, Amplitude Control of the Spin-Triplet Supercurrent in S/F/S Josephson Junctions. *Phys. Rev. Lett.* **116**, 077001 (2016).
- [30] J. A. Glick, V. Aguilar, A. B. Gougam, B. M. Niedzielski, E. C. Gingrich, R. Loloee, W. P. Pratt Jr., and N. O. Birge, Phase control in a spin-triplet SQUID. *Sci. Adv.* **4**, eaat9457 (2018).
- [31] K. Lahabi, M. Amundsen, J. A. Ouassou, E. Beukers, M. Pleijster, J. Linder, P. Alkemade, and J. Aarts. Controlling supercurrents and their spatial distribution in ferromagnets. *Nature Commun.* **8**, 2056 (2017).
- [32] O. Vávra, R. Soni, A. Petraru, N. Himmel, I. Vávra, J. Fabian, H. Kohlstedt, and Ch. Strunk, Coexistence of tunneling magnetoresistance and Josephson effects in SFIFS junctions. *AIP Adv.* **7**, 025008 (2017).
- [33] D. Lenk, V. I. Zdravkov, J.-M. Kehrle, G. Obermeier, A. Ullrich, R. Morari, H.-A. Krug von Nidda, C. Müller, M. Yu. Kupriyanov, A. S. Sidorenko, S. Horn, R. G. Deminov, L. R. Tagirov and R. Tidecks, Thickness dependence of the triplet spin-valve effect in superconductor-ferromagnet-ferromagnet heterostructures. *Beilstein J. Nanotechnol.* **7**, 957 (2016).
- [34] O. M. Kapran, A. Iovan, T. Golod, and V. M. Krasnov, Observation of the dominant spin-triplet supercurrent in Josephson spin valves with strong Ni ferromagnets. *Phys. Rev. Research* **2**, 013167 (2020).
- [35] J. P. Cascales, Y. Takamura, G. M. Stephen, D. Heiman, F. S. Bergeret, and J. S. Moodera, Switchable Josephson junction based on interfacial exchange field. *Appl. Phys. Lett.* **114**, 022601 (2019).
- [36] M. Weides, Magnetic anisotropy in ferromagnetic Josephson junctions, *Appl. Phys. Lett.* **93**, 052502 (2008).
- [37] A. Iovan and V. M. Krasnov, Signatures of the spin-triplet current in a Josephson spin valve: A micromagnetic analysis. *Phys. Rev. B* **96**, 014511 (2017).
- [38] I. A. Golovchanskiy, V. V. Bol'ginov, V. S. Stolyarov, N. N. Abramov, A. Ben Hamida, O. V. Emelyanova, B. S. Stolyarov, M. Yu. Kupriyanov, A. A. Golubov, and V. V. Ryazanov, Micromagnetic modeling of critical current oscillations in magnetic Josephson junctions, *Phys. Rev. B* **94**, 214514 (2016).
- [39] M. A. E. Qader, R. K. Singh, S. N. Galvin, L. Yu, J. M. Rowell, N. Newman, Switching at small magnetic fields in Josephson junctions fabricated with ferromagnetic barrier layers. *Appl. Phys. Lett.* **104**, 022602 (2014).
- [40] S.V. Bakurskiy, N.V. Klenov, I. I. Soloviev, M. Yu. Kupriyanov and A. A. Golubov, Superconducting phase domains for memory applications. *Appl. Phys. Lett.* **108**, 042602 (2016).
- [41] S.V. Bakurskiy, N. V. Klenov, I. I. Soloviev, N. G. Pugach, M. Yu. Kupriyanov and A. A. Golubov, Protected  $0 - \pi$  states in SIFS junctions for Josephson memory and logic. *Appl. Phys. Lett.* **113**, 082602 (2018).
- [42] S. E. Shafraniuk, I. P. Nevirkovets and O. A. Mukhanov, Modeling Computer Memory Based on Ferromagnetic/Superconductor Multilayers. *Phys. Rev. Applied* **11**, 064018 (2019).
- [43] N. Klenov, Y. Khaydukov, S. Bakurskiy, R. Morari, I. Soloviev, V. Boian, T. Keller, M. Kupriyanov, A. Sidorenko and B. Keimer, Periodic Co/Nb pseudo spin valve for cryogenic memory. *Beilstein J. Nanotechnol.* **10**, 833–839 (2019).
- [44] A.V. Samoilov, A. Legris, F. Rullier-Albenque, P. Lejay, B. Bouffard, Z.G. Ivanov and L.-G. Johansson. Mixed-State Hall Conductivity in High- $T_c$  Superconductors: Direct Evidence of Its Independence on Disorder *Phys. Rev. Lett.* **74** 2351 (1995).
- [45] V. M. Krasnov and G.Yu. Logvenov, Selfconsistent analysis of Magnus and thermal forces acting on vortices in type-II superconductors. *Physica C* **274**, 286-294 (1997).
- [46] E. B. Sonin, Magnus force in superfluids and superconductors. *Phys. Rev. B* **55**, 485-501 (1997).
- [47] The measured Hall signal contains some add mixture of the longitudinal resistance. We did not remove it from the data because it does not prevent observation of nonlinear bias-dependent effects associated with vortex motion.
- [48] R. Laiho, E. Lähderanta, E. B. Sonin, and K. B. Traito, Penetration of vortices into the ferromagnet/type-II superconductor bilayer. *Phys. Rev. B* **67**, 144522 (2003).
- [49] V. K. Vlasko-Vlasov, U. Welp, A. Imre, D. Rosenmann, J. Pearson, and W. K. Kwok, Soft magnetic lithography and giant magnetoresistance in superconducting/ferromagnetic hybrids. *Phys. Rev. B* **78**, 214511 (2008).
- [50] A. Yu. Aladyshkin, A. V. Silhanek, W. Gillijns and V. V. Moshchalkov, Nucleation of superconductivity and vortex matter in superconductor–ferromagnet hybrids. *Supercond. Sc. Technol.* **22**, 053001 (2009).
- [51] M. Iavarone, A. Scarfato, F. Bobba, M. Longobardi, G. Karapetrov, V. Novosad, V. Yefremenko, F. Giubileo, and A. M. Cucolo, Imaging the spontaneous formation of vortex-antivortex pairs in planar superconductor/ferromagnet hybrid structures. *Phys. Rev. B* **84**, 024506 (2011).
- [52] M. Flokstra, J. M. van der Knaap, and J. Aarts, Magnetic coupling in superconducting spin valves with strong ferromagnets. *Phys. Rev. B* **82**, 184523 (2010).
- [53] F. Béron, D. Ménard, and A. Yelon, First-order reversal curve diagrams of magnetic entities with mean interaction field: A physical analysis perspective. *J. Appl. Phys.* **103**, 07D9088 (2008).
- [54] C.-I. Dobrotă and A. Stancu, What does a first-order reversal curve diagram really mean? A study case: Array of ferromagnetic nanowires. *J. Appl. Phys.* **113**, 043928 (2013).
- [55] R. K. Dumas, P. K. Greene, D. A. Gilbert, L. Ye, C. Zha, J. Åkerman, and K. Liu, Accessing different spin-disordered states using first-order reversal curves. *Phys. Rev. B* **90**, 104410 (2014).